Diffusion by extrinsic noise in a two-dimensional anisotropic web mapping

Gunyoung Park[1] and C. S. Chang[1,2]

[1]*Physics Department, Korea Advanced Institute of Science and Technology, 373-1 Kusong-dong, Yuseong-ku, Taejon 305-701, Korea*
[2]*Courant Institute of Mathematical Sciences, New York University, New York, New York 10012*

Diffusion by an extrinsic noise is studied in a two-dimensional anisotropic web mapping where the intrinsic web diffusion is negligible, diffusion in one direction is dominant over the other, and the extrinsic noise enters in the dominant dimension only. It is found that the diffusion scaling is governed by the competition between the extrinsic noise and the intrinsic rotation. If the extrinsic noise is weaker than the intrinsic rotation, diffusion scales as $lK^{1/2}$ in the dominant direction and as $lK^{3/2}$ in the nondominant direction, where l is the extrinsic noise strength and K is the intrinsic perturbation parameter. If the extrinsic noise is stronger, diffusion behaves as $l^2/2$ in the dominant direction and as $K^2/4$ in the nondominant direction. Diffusion in the nondominant direction can be important if the equilibrium system is translationally invariant in the dominant direction.

I. INTRODUCTION

Effect of extrinsic noise on global diffusion in nonlinear dynamical systems is an important problem. In the so-called standard mapping, represented by

$$P_{n+1} = P_n + K \sin \varphi_n$$

and

$$\varphi_{n+1} = \varphi_n + P_{n+1},$$

for two variables P and φ with the intrinsic perturbation parameter K, the basic structure of the phase space is anisotropic. Below the stochasticity threshold, regions of intrinsic stochasticity and regions dominated by KAM (Kol'mogorov-Arnol'd-Moser) curves are infinitely extended in the φ direction, but localized and alternate in the P direction [1]. The fast diffusion in the P direction by the intrinsic stochasticity is then blocked by the KAM-dominant regions. In this case, the extrinsic noise enhances the global diffusion by letting the phase points "leak" across the KAM-dominant regions [2]. Above the stochasticity threshold, on the other hand, the region of intrinsic stochasticity extends infinitely in both directions and provide global diffusion. In this case, the extrinsic noise reduces the global diffusion by moving the phase points into and out of the KAM islands [3].

When a linear oscillator is resonantly perturbed, we can have an isotropic "web" mapping where the phase space is divided into infinitely periodic two-dimensional tiles. Within the tiles, the phase points rotate along the KAM curves. The separatrix between the tiles usually forms a connected, stochastic web structure, which yields a fast global diffusion for phase points within the stochastic web. If the intrinsic perturbation is reasonably strong and the web diffusion is fast, the extrinsic noise slows down the global web diffusion by moving the phase points into and out of the KAM tile regions. The reduction in the diffusion rate is given by the ratio of phase-space areas of intrinsic to extrinsic stochasticity [3]. If the intrinsic web diffusion is weak then the diffusion can be dominated by the extrinsic mechanism. Reference [3] studied this mechanism, however, without a satisfactory un-

derstanding of the numerical findings. Their analytic calculation showed that the diffusion is proportional to the extrinsic noise strength (l), independent of the intrinsic perturbation strength (K), while their numerical result showed an indisputable K dependence in the diffusion coefficient. In Ref. [4] we have shown analytically that the diffusion has $lK^{1/2}$ dependence, which agrees with the numerical result. These results sum up the effect of extrinsic noise on the isotropic web mapping.

When we add a toggle factor in the above standard mapping equations (which are anisotropic)

$$P_{n+1} = P_n + K \sin \varphi_n \quad \text{and}$$

$$\varphi_{n+1} = \varphi_n + (-1)^n P_{n+1},$$

the mapping changes into another type of web mapping that is anisotropic in the phase space [5]. In Fig. 1 we show the phase-space structure of this mapping. Owing to the
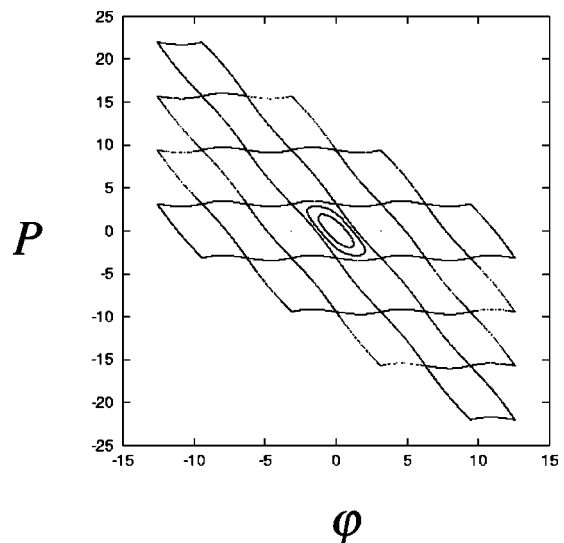
FIG. 1. Phase-space structure of Eq. (2) with $l=0$ in the limit $K \to 0$, where connected separatrix network is given by $\cos \varphi + \cos(\varphi + P) = 0$. P and φ are in radians.

"toggle" factor $(-1)^n$ in the second equation, we call it the "toggle mapping." This is an area preserving web mapping that is anisotropic in P and φ. Properties of the intrinsic global web diffusion in the above anisotropic web mapping is not much different from the usual isotropic web mapping. In this report, we study the effect of the extrinsic noise on the anisotropic web mapping using the above toggle mapping equations. The physical situation in Ref. [5] demands that the unperturbed system is translationally invariant in the φ direction and the external noise explicitly scatters only φ values. The variable P then suffers scattering through coupling with φ:

$$P_{n+1} = P_n + K \sin \varphi_n,$$

$$\varphi_{n+1} = \varphi_n + (-1)^n P_{n+1} + l\xi, \tag{1}$$

where $l\xi$ is the extrinsic noise, l is the noise strength, and ξ is taken here to be a normal distribution of random variable with variance = 1 and mean = 0. We note here that we may take ξ to be a uniformly distributed random variable, without changing the conclusion of the present work.

II. NUMERICAL RESULTS

The discrete mapping Eq. (1) are studied numerically. In order to measure the diffusion coefficient, a single orbit is broken into N pieces and each of them has T mapping steps. Thus, the total length of the single orbit is NT. Numerical diffusion coefficient for P (or φ) is then given by

$$D_P = \frac{1}{N} \sum_{i=1}^{N} \frac{1}{2T} (P_i - P_{(i-1)})^2.$$

Here, T must be sufficiently large to insure that the transient behavior dies out, and N must be large enough to provide meaningful statistics. These conditions are satisfied by choosing T and N to be 2 000 000 and 1000, respectively, in the present work.

We first examine the diffusion D_φ in the dominant direction φ. Figure 2 shows the dependence of D_φ on the noise coefficient l for three different values of the intrinsic perturbation K. It can be seen that D_φ increases in proportion to l at lower l values and to l^2 at higher l values with the curves collapsing into one. The boundary between these two slopes becomes lower at lower K value, being proportional to $K^{1/2}$. The dependence of D_φ on K is examined in Fig. 3 for three different values of l. The slope is about K^0 at lower K, but about $K^{1/2}$ at higher K. The boundary between the two slopes increases in proportion to l^2. These observations lead to two different diffusion scalings with the transition boundary behaving like $l/K^{1/2}$, suggesting that the diffusions at each side of the boundary are led by different physical processes.

We next examine the diffusion D_P in the nondominant direction P. Figure 4 shows the dependence of D_P on the noise coefficient l for three different values of the intrinsic perturbation K. D_P increases in proportion to l at lower l values, but shows plateau behavior at higher l values. As in the above D_φ case the l boundary between these two slopes
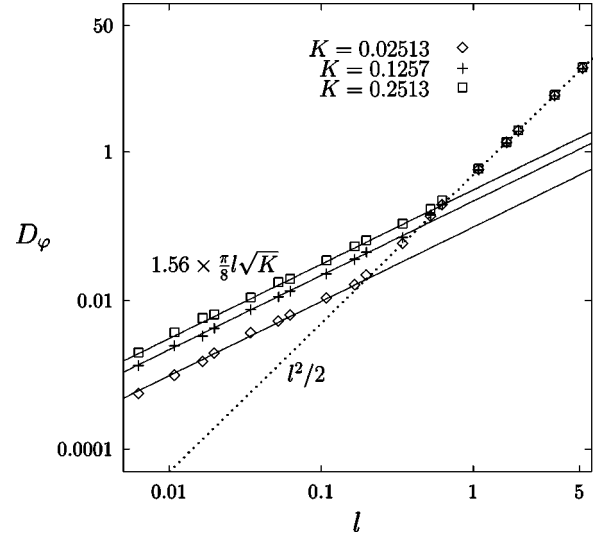
FIG. 2. Plot of D_φ(radian^2/mapping step) vs l. The marks $\Diamond$ ($K=0.025\,13$), $+$ ($K=0.1257$), and $\Box$ ($K=0.2513$) show numerical results. The solid lines are from formula $D_\varphi=1.56 \times (\pi/8)l\sqrt{K}$ and the dotted line is from $D_\varphi=l^2/2$.

is proportional to $K^{1/2}$. The dependence of D_P on K is examined in Fig. 5 for three different values of l. The slope is about K^2 at lower K, but about $K^{3/2}$ at higher K. The K transition boundary between the two slopes increases in proportion to l^2. These observations again suggest two different diffusion scalings with the transition boundary behaving like $l/K^{1/2}$.

From extensive numerical investigations, including Figs. 2–5, it is observed that a normalized extrinsic noise strength $\hat{l} \propto l/K^{1/2}$ is a meaningful parameter in the description of the diffusion process. Numerical diffusion at $\hat{l}<1$ scales differ-
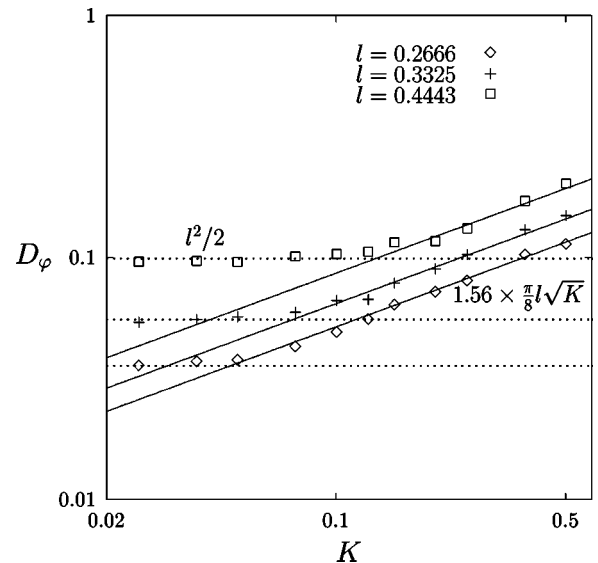
FIG. 3. Plot of D_φ(radian^2/mapping step) vs K. The marks $\Diamond$ ($l=0.2666$), $+$ ($l=0.3325$), and $\Box$ ($l=0.4443$) show numerical results. The solid lines are from formula $D_\varphi=1.56 \times (\pi/8)l\sqrt{K}$ and the dotted line is from $D_\varphi=l^2/2$.
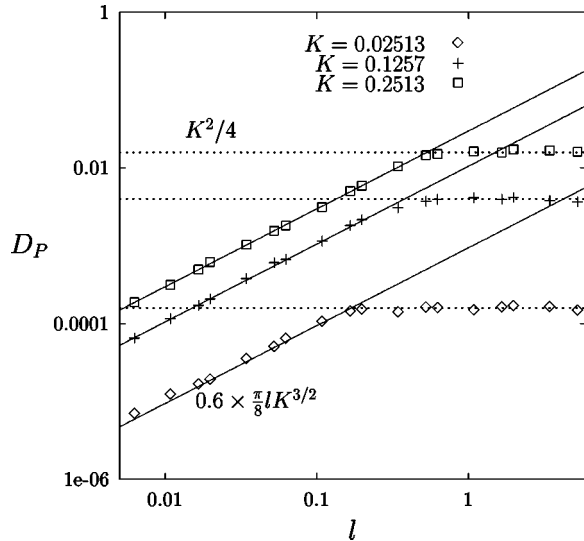
FIG. 4. Plot of D_P (radian^2/mapping step) vs l. The marks $\Diamond$ ($K=0.025\,13$), $+$ ($K=0.1257$), and $\square$ ($K=0.2513$) show numerical results. The solid lines are from formula $D_P=0.6 \times (\pi/8)lK^{3/2}$ and the dotted line is from $D_P=K^2/4$.

ently from that at $\hat{l}>1$. We now present a simplified analytic description of the noisy diffusion processes in the intrinsically quiescent toggle mapping, which can provide us a basic understanding of the l and K scaling, and the boundary parameter $\hat{l} \propto l/K^{1/2}$.

III. ANALYTIC EVALUATION OF THE DIFFUSION COEFFICIENTS

For an analytic evaluation, it is more convenient to convert Eq. (1) into the following equivalent form:

$$P_{n+2}=P_n+K\sin\varphi_n+K\sin[\varphi_n+P_n+K\sin\varphi_n+l\xi_1],$$
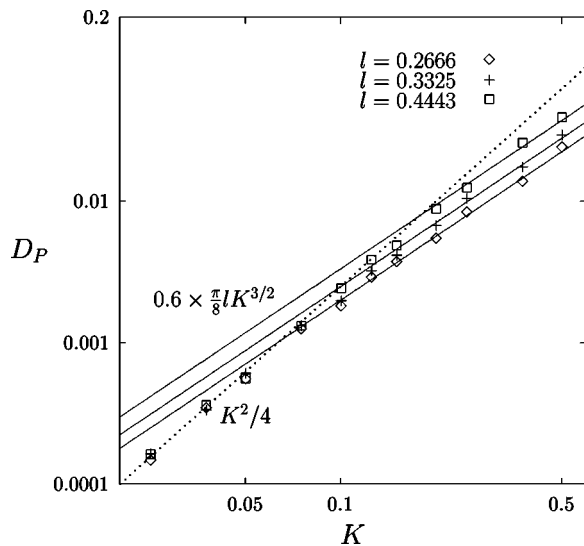
FIG. 5. Plot of D_P (radian^2/mapping step) vs K. The marks $\Diamond$ ($l=0.2666$), $+$ ($l=0.3325$), and $\square$ ($l=0.4443$) show numerical results. The solid lines are from formula $D_P=0.6\times(\pi/8)lK^{3/2}$ and the dotted line is from $D_P=K^2/4$.
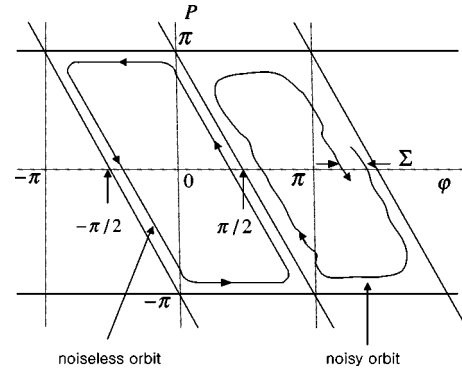
FIG. 6. Cartoon sketch of the orbit trajectories with and without noise effects. Σ indicates the mismatch of the orbit for the case $l\neq0$.

$$\varphi_{n+2}=\varphi_n-K\sin[\varphi_n+P_n+K\sin\varphi_n+l\xi_1]+l(\xi_1+\xi_2),$$
$$(2)$$

where ξ_1 and ξ_2 are two independent random numbers and the $(n+1)$th step is suppressed to remove the toggle factor in the φ equation. A cartoon picture for phase-space structure of Eq. (2) is shown in Fig. 6. The K number is chosen to be small enough to have a negligible internal separatrix stochasticity. During one complete rotation along a KAM curve within the tile, the phase point experiences external noise that scatters the phase point off the unperturbed orbit. The scattered phase point no longer has closed orbit, resulting in a mismatch Σ in the φ direction after one complete rotation motion. The size of Σ can be estimated from a random walk argument,

$$\Sigma \simeq lN_0^{1/2},$$

where N_0 is the number of mapping steps per complete rotation within the tile in the absence of the extrinsic noise. Since the length of the intrinsic rotation motion per one mapping step is $\propto K$, N_0 is proportional to $1/K$. In general N_0 is a function of orbital position within the tile. For a qualitative description, however, we use a simplified N_0 here, $N_0\simeq\lambda/K$, where λ is a constant to be determined later when we compare the analytic result with the numerical simulation. Thus, Σ becomes

$$\Sigma \simeq \lambda^{1/2}l/K^{1/2}. \qquad (3)$$

Since the half-width of the unit tile in the φ direction is $\pi/2$ (See Fig. 6), there can be two different types of diffusions depending upon the magnitude of Σ relative to $\pi/2$. If $\Sigma \gg \pi/2$, the strong extrinsic noise can detrap a phase point out of a tile before the completion of an internal rotation. If $\Sigma \ll \pi/2$ then the phase point experiences rotations before detrapping by weak extrinsic noise. Let us first consider the weak extrinsic noise case, $\Sigma \ll \pi/2$. If we define a normalized extrinsic noise parameter $\hat{l}=2\lambda^{1/2}l/\pi K^{1/2}$, then the weak extrinsic noise regime is represented as $\hat{l}\ll1$. We partition a tile in Fig. 6 along φ axis ($P=0$) from zero to $\pi/2$ into n discrete cells as shown in Fig. 7. The size of a cell is taken to be Σ. A phase point initially at the kth cell can scatter by the
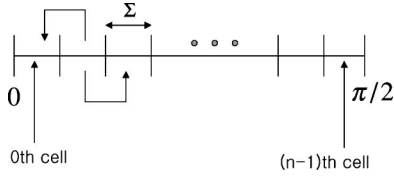
FIG. 7. Partitioning of a tile into n cells along the $P=0$ axis of Fig. 6 between $\varphi=0$ and $\pi/2$.

extrinsic noise either into $(k+1)$th or $(k-1)$th cell after one rotation. In Fig. 7 the 0th cell corresponds to the center of the unit tile, which is bounded by a perfectly reflecting boundary. The $(n-1)$th cell represents the last one before detrapping into the neighboring tile (nth cell): Thus, the nth cell is an absorbing boundary.

We now evaluate the average detrapping time out of a tile. The relevant quantity here is the mean number of rotations C_k before the phase point hits the absorbing boundary at the nth cell starting from the kth cell. Transition probability to the right (left) cell is denoted as p (q). Let $P(T|s=k)$ be the probability for the phase point initially at the kth cell to reach the absorbing boundary after T rotational steps. The recursion equation for C_k $(1\leqslant k\leqslant n-1)$ can, then, be obtained as follows:

$$C_k = \sum_{T=1}^{\infty} P(T|s=k)T$$

$$= \sum_{T=1}^{\infty} T[pP(T-1|s=k+1)+qP(T-1|s=k-1)]$$

$$= p\sum_{T=2}^{\infty} TP(T-1|s=k+1)+q\sum_{T=2}^{\infty} TP(T-1|s=k-1)$$

$$= p[1+C_{k+1}]+q[1+C_{k-1}]=1+pC_{k+1}+qC_{k-1}, \quad (4)$$

where $p+q=1$ and $\Sigma_{T=1}^{\infty}P(T|s=k\pm1)=1$ have been used. Since the extrinsic noise in the present work does not prefer right or left transitions, we assume $p=q=1/2$. Under the appropriate boundary conditions, $C_n=0$ and $C_0=1+C_1$, an appropriate solution to Eq. (4) is obtained as (see Ref. [4])

$$C_k=n^2-k^2.$$

For a time asymptotic behavior we need to consider the average detrapping time of a newly migrated phase point starting its activity within the tile at the $(n-1)$th cell. Thus, k is $n-1$ and $C_{n-1}=2n-1\simeq2n\simeq\pi/\Sigma$. The average detrapping time τ_{av} in a tile is, therefore, given as

$$\tau_{av}=C_{n-1}N_0\simeq\frac{\pi}{\Sigma}N_0\simeq\frac{\pi}{l}\left(\frac{\lambda}{K}\right)^{1/2}. \quad (5)$$

Before proceeding to the evaluation of the diffusion coefficient, a numerical calculation of the τ_{av} is performed in order to compare with the analytic expression (5). The result is shown in Fig. 8. The + and $\diamond$ marks are numerical simulation results for $K=0.1257$ and 0.025 13, respectively. The simple analytic prediction of Eq. (5) is shown as straight
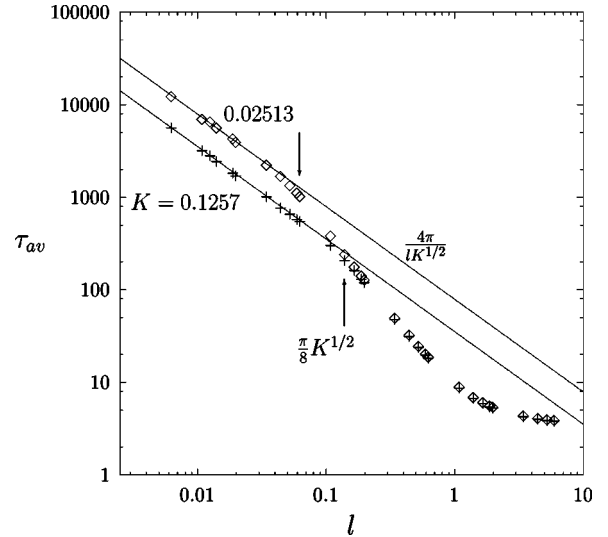
FIG. 8. Plot of average detrapping time τ_{av} in mapping steps as a function of l. $K=0.1257$ (+ marks) and 0.025 13 ($\diamond$ marks) are chosen. $\diamond$ and + mark the numerical results and the solid lines are from Eq. (5) with $\lambda^{1/2}=4$. The arrows mark the location of $l=\pi K^{1/2}/8$.

lines. It is found that $\lambda^{1/2}=4$ yields an excellent fit of the analytic formula to the numerical result in the small extrinsic noise regime ($\hat{l}<1$). The abrupt change of the numerical τ_{av} behavior around $\hat{l}=8l/(\pi K^{1/2})=1$ supports the validity of the $\hat{l}$ parameter.

Using this expression for τ_{av} we can obtain the diffusion coefficient D_{φ} in the dominant direction φ from a random walk formula,

$$D_{\varphi}\simeq\frac{\pi^2}{2\tau_{av}}\simeq\frac{\pi}{8}l\sqrt{K}, \quad (6)$$

where π is the random walk step size, corresponding to the distance between the centers of the neighboring tiles in the φ direction. At this point we would like to mention that the tile to tile transition dynamics is not completely random, as pointed out in Refs. [4] and [6], but the correlation over consecutive transition steps exists because the exit direction to the next tile is likely to be affected by the entrance direction into the present tile. This point can be easily understood by using Fig. 9, where α denotes the forward transition probability (parallel to the entering direction) and β does the backward transition probability (opposite to the entering direction). Due to the natural convective rotation within a tile, a newly immigrated phase point across a separatrix meets the opposite separatrix (where a forward transition is possible) before it comes back to the entry side separatrix. Thus α is greater than β. Here we note that the transition probability in the P direction is small compared to that in the φ direction in the small K limit as can be easily understood from the form of Eqs. (1) or (2). This correlation effect usually enhances the numerical coefficient with a correction coefficient of order unity [7], but does not alter the diffusion scaling with respect to K and l. Considering that the present analytic work
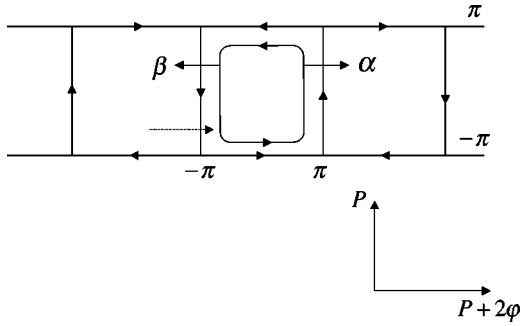
FIG. 9. Diagram defining cell to cell transition probabilities α and β. Dotted arrow indicates entrance and solid arrows do exit direction. Direction of natural convective motions is also indicated.

is rather qualitative in nature, such an elaboration is not necessary and will not be pursued. We now analyze the diffusion in the nondominant direction, D_P.

Let us remember that the relative probability f_P of transition in the P direction compared to that in the φ direction is quite weak. The quantity f_P may be defined as $f_P \equiv \Delta P/(2\Delta\varphi)$, where $\Delta P(\Delta\varphi)$ is the size of the displacement per two mapping steps [n to $n+2$ in Eq. (2)] induced by the extrinsic noise l in the $P(\varphi)$ direction. The factor 2 is multiplied in the denominator to compensate for the difference (2π vs π) in the tile size between the P and φ directions (see Fig. 6). It is trivial to obtain $\Delta\varphi = \sqrt{2}l$ from Eq. (2). To find ΔP we express the difference $P_{n+2} - P_n$ of Eq. (2) in the following form:

$$P_{n+2} - P_n = K\sin[\varphi_n] + K\sin[\varphi_n + P_{n+1}]$$
$$+ K\cos[\varphi_n + P_{n+1}]\sin[l\xi_1]$$
$$+ K\sin[\varphi_n + P_{n+1}]\{\cos[l\xi_1] - 1\}. \quad (7)$$

We then calculate the effect of the extrinsic noise on $P_{n+2} - P_n$ along the unperturbed orbit, which Eq. (2) specifies as

$$K\sin[\varphi_n] + K\sin[\varphi_n + P_{n+1}] \simeq 0.$$

Using this relationship, Eq. (7) becomes

$$P_{n+2} - P_n \simeq -K\cos\varphi_n\sin[l\xi_1] - K\sin\varphi_n\{\cos[l\xi_1] - 1\}.$$

We square both sides and take average over φ and ξ_1. From the relationship $\langle\cos^2(\varphi)\rangle_\varphi = \langle\sin^2(\varphi)\rangle_\varphi = \frac{1}{2}$ and $\langle\sin(l\xi_1)\rangle_{\xi_1} = 0$, and $\langle\cos(l\xi_1)\rangle_{\xi_1} = \exp[-l^2/2]$ where $\langle\cdots\rangle_x$ means average over x, we find

$$\langle(P_{n+2} - P_n)^2\rangle_{\varphi,\xi_1} = K^2(1 - \langle\cos[l\xi_1]\rangle_{\xi_1})$$
$$= K^2(1 - \exp[-l^2/2])$$
$$\simeq \frac{K^2}{2}l^2, \quad \text{for} \quad l \ll 1.$$

Thus, ΔP becomes

$$\Delta P = \sqrt{\langle(P_{n+2} - P_n)^2\rangle_{\varphi,\xi_1}} = lK/\sqrt{2}.$$

The relative transition probability $f_P = \Delta P/(2\Delta\varphi)$ is, then, $K/4$. The diffusion in the P direction in the limit $\hat{l} \ll 1$, which takes the random walk size of 2π per detrapping, becomes

$$D_P = f_P\frac{(2\pi)^2}{2\tau_{av}} = \frac{\pi}{8}lK^{3/2}, \quad (8)$$

which is smaller than D_φ by a factor K as can be qualitatively anticipated from the structure of the mapping equation (1) or (2). Note here that the regime $\hat{l} \ll 1$ may be regarded as the spatial correlation regime because, although extrinsic noise modifies the unperturbed orbit trajectory, the overall form of orbit trajectories maintains the rotational structure.

In the extrinsically noisy regime $\hat{l} \gg 1$ (or equivalently $\Sigma \gg \pi/2$), the above analysis based upon the existence of rotational orbits, does not apply since the orbits are destroyed before completion of a rotation. However, a theory based upon the complete decorrelation may not guarantee the correct result here because the time series of the mapping trajectory may be temporally correlated as long as the l is less than unity. Two alternative methods have been developed previously to include the time correlation effects [2]: Fourier-space paths and characteristic function methods. In the present discussion we choose the Fourier-space paths method to derive the diffusion coefficient in the extrinsically noisy regime.

The Fourier-space paths method was originally introduced in Ref. [8] and a general description of its methodology has appeared in Ref. [2]. Application of this method to the problem of diffusive heating by lower hybrid waves has appeared in Refs. [9] and [10]. In this method we define a distribution function $W(P,\varphi,n|P_0,\varphi_0,0)$ of the phase points as a function of the position (P,φ) at the mapping time n for a given initial position (P_0,φ_0) at time 0, and define its Fourier transform $a_n(m_n,q_n)$:

$$a_n(m_n,q_n) = \frac{1}{(2\pi)^2}\int d\varphi dP e^{-im_n\varphi - iq_nP}$$
$$\times W(P,\varphi,n|P_0,\varphi_0,0). \quad (9)$$

It is shown in Refs. [2] and [8], using a standard mapping equation, that the time asymptotic diffusion coefficient

$$D_P = \lim_{n\to\infty} D_{Pn} = \lim_{n\to\infty}\frac{\langle(P_n - P_0)^2\rangle}{2n}$$

can be expressed in terms of the second derivative of a_n at the origin of the Fourier space ($m = 0, q = 0+$):

$$D_{Pn} = -\frac{4\pi^2}{2n}\frac{\partial^2[a_n(0,q)e^{iqP_0}]}{\partial q^2}\bigg|_{q=0+}. \quad (10)$$

Here $q = 0+$ is used here for convenience only. This method requires the sign of q at all times, as will become obvious soon (see Appendices). It is also shown that the function $a_n(m,q)$ at the origin is obtained from the recursion relation for $a_n(m_n,q_n)$,

$$a_n(m_n, q_n) = \sum_{j_n} J_{j_n}(|q_{n-1}|K) a_{n-1}(m_{n-1}, q_{n-1}) e^{-m_n^2 l^2/2}$$

$$(11)$$

by iterating backward in time using the selection rules

$$m_{n-1} = m_n + j_n \, \mathrm{sgn}(q_{n-1}),$$

$$q_{n-1} = q_n + (-1)^n m_n, \qquad (12)$$

to choose the proper paths in the Fourier space. Basic methods to derive the diffusion formula (10), recursion relation (11), and selection rules (12) are the same as those in Refs. [2] and [8], which developed the methods for the standard mapping [without the toggle factor $(-1)^n$ in our mapping]. For the sake of completeness, we present these derivations in Appendix A.

In the Appendix A, it is also shown that the diffusion coefficient in the dominant direction φ can be expressed in the symmetric way to Eq. (10):

$$D_\varphi = \lim_{n \to \infty} D_{\varphi_n} = \lim_{n \to \infty} \frac{\langle (\varphi_n - \varphi_0)^2 \rangle}{2n},$$

and

$$D_{\varphi_n} = -\frac{4\pi^2}{2n} \frac{\partial^2 [a_n(m, 0+) e^{im\varphi_0}]}{\partial m^2} \bigg|_{m=0}. \qquad (13)$$

There are countless proper Fourier paths satisfying the selection rules. Each Fourier path is associated with the corresponding set of $\{j_i\}$. All these Fourier-space paths must be summed up to obtain accurate $a_n(0,0+)$, which is practically impossible. Instead, we obtain an approximate expression for $a_n(0,0+)$ by taking the dominant Fourier-space paths that gives the lowest-order contributions. It is shown in Appendix B that the dominant contribution to $a_n(m,q)|_{m=0, q=+0}$ comes from the paths staying at the origin of the Fourier space forever, to yield

$$a_n(m,q) = \frac{1}{4\pi^2} [J_0(qK) e^{-m^2 l^2/2}]^n e^{-iqP_0} e^{-im\varphi_0}$$

$$\text{for} \quad m \to 0, q \to +0. \quad (14)$$

Equations (10) and (13) then yield

$$D_P = K^2/4 \quad \text{and} \quad D_\varphi = l^2/2. \qquad (15)$$

Surprisingly, these are what we would obtain from the random phase assumption in Eq. (1):

$$D_P = \frac{1}{2} \langle (P_{n+1} - P_n)^2 \rangle_{\varphi_n} = \frac{1}{4\pi} \int_0^{2\pi} K^2 \sin^2 \varphi \, d\varphi = \frac{K^2}{4},$$

and
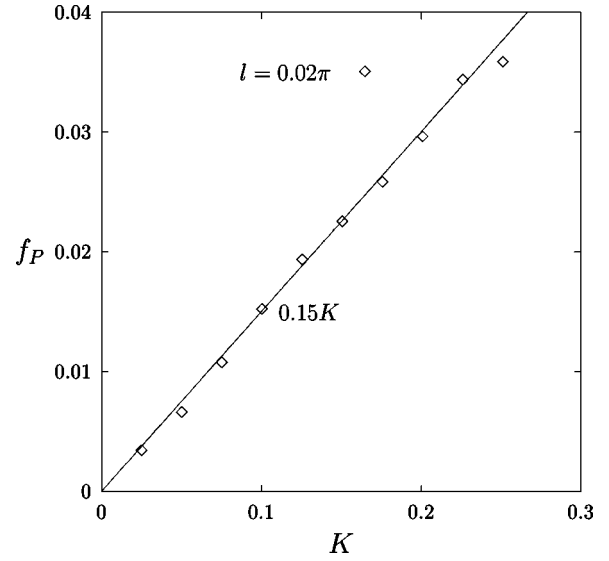
FIG. 10. The relative transition probability f_P as a function of K for $l = 0.02\pi$. The points are numerical values, whereas the line is $f_P = 0.15K$.

$$D_\varphi = \frac{1}{2} \langle (\varphi_{n+1} - \varphi_n)^2 \rangle_\xi$$

$$= \frac{1}{2\sqrt{2\pi}} \int_{-\infty}^{\infty} l^2 \xi^2 e^{-\xi^2/2} d\xi = \frac{1}{2} l^2,$$

where $\langle \cdots \rangle_X$ means average over X. The only difference between the present derivation in the Appendix B and that in Refs. [2] and [8] is in the modification of the Fourier paths due to the toggle factor. However, this minor difference brings out a major difference in the result: The present result (15) turns out to be equivalent to the diffusion coefficient under the random phase assumption, while the corresponding result without the toggle factor is not [2,8]. It may be important to realize that, although we have $l < 1$, it is found here that the toggle factor can wipe out the temporal correlation, making the diffusion obey the random phase dynamics.

The analytic results are compared with the numerical simulation results. Earlier in this report, comparison of the analytic detrapping time τ_{av} with the numerical result was presented in Fig. 8, where an excellent agreement in the l dependence allowed us to determine the proportionality constant λ in the weak extrinsic noise regime. Figure 10 compares the transition probability ratio f_P. Numerical result shows $f_P = 0.15K$, while the analytic result is $f_P = 0.25K$. This is a reasonable agreement considering the qualitative nature of the present analytic theory.

Diffusion coefficients in the dominant direction φ are compared in Figs. 2 and 3 as function of l and K, respectively, where the correction coefficient, as mentioned before, is found numerically to be given as 1.56. The agreement between the simulation and analytic diffusion is excellent in φ direction. Diffusion coefficient in the nondominant direction D_P is compared in Figs. 4 and 5. Except for a minor adjustment in the proportionality constant in the analytic formula due to the difference between the numerical

f_P (0.15K) and the analytic f_P (0.25K), an excellent agreement with the simulation results in the l and K dependences is verified in the both weak and strong extrinsic noise regimes. Two distinctive scalings of D_P with respect to l and K, which are separated around the point $\hat{l}=8l/(\pi K^{1/2})\simeq 1$, are verified both numerically and analytically. In fact, all the features of the analytic understanding agree with the numerical observations.

IV. CONCLUSION

In the present work we have studied diffusion phenomena driven by extrinsic noise in a two-dimensional anisotropic web mapping in which the two-dimensional variables play different roles with respect to each other. The first variable is changed by a small intrinsic perturbation K, and the second variable is varied by the changes in the first variable with a toggle factor and an extrinsic noise with the strength l. The phase of the intrinsic perturbation is determined by the changes in the second variable. The mapping is different from the standard mapping due to the presence of the toggle factor. A dominant diffusion then occurs in the extrinsically noisy, second direction (dominant direction). The intrinsic stochastic web diffusion is assumed to be negligible. It is found that the diffusion mechanism is governed by the competition between the extrinsic noise frequency and the intrinsic rotation frequency. If the extrinsic frequency is slower than the intrinsic frequency, diffusion scales as $lK^{1/2}$ in the dominant direction and as $lK^{3/2}$ in the nondominant direction. If the extrinsic frequency is stronger, diffusion behaves as $l^2/2$ in the dominant direction and as $K^2/4$ in the nondominant direction.

We understand the numerical results analytically: The simulation results agree well with the analytic results. One particularly interesting result is that the toggle factor changes the fundamental nature of the mapping: The temporal correlation, which exists without the toggle factor, is destroyed. Thus, when the spatial correlation is destroyed by a stronger extrinsic noise frequency than the rotation frequency, the diffusion obeys the random phase dynamics due to the destruction of the temporal correlation by the toggle factor. The results presented here for the nondominant directional diffusion can be important in the case when the dominant direction is translationally invariant in equilibrium. In this case the diffusion in the nondominant direction determines the loss process of a physical system.

APPENDIX A: DIFFUSION FORMULA, RECURSION RELATION, AND SELECTION RULE FOR THE FOURIER-PATH METHOD

The derivations given here are parallel to those in Ref. [2] except for the minor modification caused by the toggle factor

$(-1)^n$ in Eq. (1). We first derive the diffusion formula (10), by substituting

$$W(P,\varphi,n|P_0,\varphi_0,0)=\int dm_n dq_n e^{im_n\varphi+iq_n P}a_n(m_n,q_n)$$

into

$$D_{Pn}=\frac{1}{2n}\int dP d\varphi W(P,\varphi,n|P_0,\varphi_0,0)P^{*2},\quad \text{and}$$

$$D_{\varphi_n}=\frac{1}{2n}\int dP d\varphi W(P,\varphi,n|P_0,\varphi_0,0)\varphi^{*2},$$

where $P^*=P-P_0$ and $\varphi^*=\varphi-\varphi_0$, we obtain

$$D_{Pn}=\int dm_n dq_n \frac{1}{2n}e^{im_n\varphi_0+iq_n P_0}\int dP^* d\varphi^* P^{*2}$$
$$\times e^{im_n\varphi^*+iq_n P^*}a_n(m_n,q_n),\qquad (A1)$$

$$D_{\varphi_n}=\int dm_n dq_n \frac{1}{2n}e^{im_n\varphi_0+iq_n P_0}\int dP^* d\varphi^* \varphi^{*2}$$
$$\times e^{im_n\varphi^*+iq_n P^*}a_n(m_n,q_n).\qquad (A2)$$

In Eq. (A1), integration over φ^* annihilates the m_n contributions except for $m_n=0$. In Eq. (A2) integration over P^* annihilates the q_n contributions except for $q_n=0$. Using $\partial^2 e^{iqP}/\partial q^2=-P^2 e^{iqP}$ and integrating by parts twice, we have

$$D_{Pn}=-\frac{2\pi}{2n}\int dP^* dq_n e^{iq_n P^*}\frac{\partial^2}{\partial q_n^2}[a_n(0,q_n)e^{iq_n P_0}],$$

$$D_{\varphi_n}=-\frac{2\pi}{2n}\int d\varphi^* dm_n e^{im_n\varphi^*}\frac{\partial^2}{\partial m_n^2}[a_n(m,0+)e^{im_n\varphi_0}].$$

Since $\int dy e^{ixy}=2\pi\delta(x)$, these equations become

$$D_{Pn}=-\frac{4\pi^2}{2n}\frac{\partial^2[a_n(0,q)e^{iqP_0}]}{\partial q^2}\bigg|_{q=0+},\quad \text{and}$$

$$D_{\varphi_n}=-\frac{4\pi^2\partial^2[a_n(m,0+)e^{im\varphi_0}]}{2n}\frac{}{\partial m^2}\bigg|_{m=0},$$

which is Eqs. (10) and (13). Setting $q=0+$ is for convenience in applying the selection rule as shown in Appendix B.

Next, we derive the recursion relation for $a_n(m_n,q_n)$ and the selection rules for (m_n,q_n). We start with the inverse Fourier transform, Eq. (9),

$$a_n(m_n,q_n)=\frac{1}{(2\pi)^2}\int d\varphi dP e^{-im_n\varphi-iq_n P}$$
$$\times W(P,\varphi,n|P_0,\varphi_0,0).\qquad (A3)$$

Using the identity relations

$$W(P,\varphi,n|P',\varphi',n-1) = \delta(P-P'-K\sin\varphi')\delta[\varphi-\varphi'$$
$$-(-1)^n(P'+K\sin\varphi')-l\xi'],$$

$$W(P,\varphi,n|P_0,\varphi_0,0)$$

$$= \int dP' d\varphi'$$

$$\times W(P,\varphi,n|P',\varphi',n-1)W(P',\varphi',n-1|P_0,\varphi_0,0),$$

where the first relation is from the mapping equation, Eq. (A3) becomes,

$$a_n(m_n,q_n) = \frac{1}{(2\pi)^2} \int d\varphi dP e^{-im_n\varphi - iq_n P} \int dP' d\varphi'$$

$$\times \delta(P-P'-K\sin\varphi')$$

$$\times \delta(\varphi-\varphi'-(-1)^n(P'+K\sin\varphi')-l\xi')$$

$$\times \int dm_{n-1}dq_{n-1}e^{im_{n-1}\varphi'+iq_{n-1}P'}a_{n-1}$$

$$\times (m_{n-1},q_{n-1}). \tag{A4}$$

Delta function integration over φ and P' leads to

$$a_n(m_n,q_n) = \frac{1}{(2\pi)^2} \int dm_{n-1}dq_{n-1}dP d\varphi'$$

$$\times e^{-im_n[\varphi'+(-1)^n P+l\xi']-iq_n P}$$

$$\times e^{im_{n-1}\varphi'+iq_{n-1}(P-K\sin\varphi')}a_{n-1}$$

$$\times (m_{n-1},q_{n-1}). \tag{A5}$$

Averaging over the random variable ξ' of normal distribution of mean=0 and variance=1, we get the factor $e^{-1/2m_n^2 l^2}$. Averaging over P produces a factor

$$2\pi\delta[q_{n-1}-(-1)^n m_n - q_n]. \tag{A6}$$

The q_{n-1} integration is then easily performed using this delta function to yield

$$a_n(m_n,q_n) = \frac{1}{2\pi} \int dm_{n-1} \int d\varphi' e^{i(m_{n-1}-m_n)\varphi'-iq_{n-1}K\sin\varphi'}$$

$$\times a_{n-1}(m_{n-1},q_{n-1})e^{-m_n^2 l^2/2}, \tag{A7}$$

where $q_{n-1}=q_n+(-1)^n m_n$. Because of the identity

$$e^{iq_{n-1}K\sin\varphi'} = \sum_{j_n=-\infty}^{\infty} J_{j_n}(|q_{n-1}|K)e^{ij_n\varphi'\,\mathrm{sgn}(q_{n-1})},$$

a subsequent integration over φ' gives another δ function

$$\delta(m_{n-1}-m_n-j_n\,\mathrm{sgn}(q_{n-1})). \tag{A8}$$

We then have

$$a_n(m_n,q_n) = \sum_{j_n} J_{j_n}(|q_{n-1}|K)a_{n-1}(m_{n-1},q_{n-1})e^{-m_n^2 l^2/2}$$

with the selection rules Eq. (12) given by the two delta functions (A6) and (A8).

APPENDIX B: DERIVATION OF EQ. (14)

In this section we derive Eq. (14), the expression for $a_n(m,q)|_{m=0,q=0+}$, by tracing the steps backward in time starting from the origin $(m=0,q=0)$ using the paths defined by Eq. (12). We show that the dominant contribution comes from the Fourier Paths staying at the origin of the Fourier-space forever. The other significant contributions cancel each other. The procedure described here is originated from the standard mapping analysis of Ref. [8], but the actual Fourier paths construction and counting are different due to the existence of the toggle factor in the present work. Naturally, the result is different.

The selection rules (12) demand a sign for q at all times including $q=0$. As long as the second derivative of $a_n(m,q)$ with respect to q is continuous at $q=0$, we can assign either sign to $q=0$. We choose $q=0+$. The selection rules (12) send the first backward path from $(m,q)=(0,0+)$ to either $(m,q)=(1,0+)$ or $(m,q)=(-1,0+)$. We can easily see that these two alternative choices produce symmetric results with respect to the $m=0$ axis. It is, thus, sufficient to analyze the backward paths with the first step to $(m,q)=(1,0+)$ only. The recursion equation (11) requires that at every step along a Fourier-space path, the Fourier component a_n decays by the factor $J_{j_i}(|q_{i-1}|K)$. Since $K\ll1$ in the present problem for a negligible intrinsic stochasticity, we have $J_j(q_{i-1}K)\sim(q_{i-1}K)^j\ll1$ and $J_0(q_{i-1}K)\simeq1-(q_{i-1}K)^2/4$. It is obvious that the lowest order contribution to $a_n(0,0+)$ comes from the Fourier-space paths that stay at the origin the whole time. Since the initial backward path out of the origin is either $(m,q)=(1,0+)$ or $(m,q)=(-1,0+)$, which requires $j=\pm1$, the path back to the origin needs at least one more step with $j=\mp1$: Thus, the next order contribution to $a_n(0,0)$ is of order K^2. It can be easily seen from a similar argument that any path going out of $|m|\leq1$ region can only contribute to $a_n(0,0+)$ at most to order K^4. We, thus, neglect any path going out of the $|m|\leq1$ region.

Within the region $|m|\leq1$, we can describe a general pattern for the path. From a point on the q axis $(m=0)$, the next path can only be to itself $(j=0)$ or vertically up and down in the m direction $(|j|=1)$. From a point away from the q axis $(m=\pm1)$ the next path can only be horizontal $(j=0)$ or diagonal $(j=\pm1)$.

One significant fact contained in Eq. (12) is that the Fourier-space path can remain stationary for any number of steps at any point on the q axis $(m=0)$, accumulating per every step the multiplication factor $J_0(|q|K)$. With these due considerations we can generate the K^2th order contributions

FIG. 11. Three different Fourier-space paths providing the K^2th order contributions to $a_n(0,q)$. Arrows indicate path direction backward in time. The j values are for Eq. (12). The filled circles at $(m,q)=(0,-1)$ indicate stationary point.

FIG. 12. Fourier-space paths extended from Fig. 11. The numbers indicate traversing order.

to $a_n(m,q)|_{m=0,q=0+}$ as shown in Fig. 11. Hereafter it is assumed, without loss of generality, that the infinitely large n is an even number. In Figs. 11(b) and 11(c) it is arranged in such a way that a part of the Fourier-space paths stay stationary at $(m,q)=(0,-1)$ for an arbitrary number of steps. $j=-1$ is chosen in Fig. 11(b) after an odd number of stationary steps and $j=1$ in Fig. 11(c) after an even number of stationary steps. These choices are necessary to have the paths to go back to the origin on the second step after the stationary point. Otherwise the Fourier-space path will turn into the negative q direction at $(m,q)=(1,-1)$ in Fig. 11(b) and at $(m,q)=(-1,-1)$ in Fig. 11(c). One can directly calculate the contributions to $a_n(0,0+)$ from the three paths depicted in Fig. 11. For Fig. 11(b) we have, after summing over all the possible odd numbered choices of steps at the stationary point,

$$\sum_{n=0}^{\infty} J_1(qK)J_1(K)J_0^{2n+1}(K)J_{-1}(K)J_{-1}(qK)e^{-l^2}$$

$$=J_1^2(qK)J_0(K)\frac{J_1^2(K)e^{-l^2}}{1-J_0^2(K)}$$

$$\simeq \frac{1}{2}J_1^2(qK)e^{-l^2} \quad \text{for} \quad K\ll 1. \quad \text{(B1)}$$

Note here that the summation over the number of stationary steps raises the magnitude from $\sim K^4$ to $\sim K^2$. The same contribution can also be obtained for the path in Fig. 11(c). On the other hand for Fig. 11(a) it is

$$J_1(qK)J_0(K)J_{-1}(qK)e^{-l^2}\simeq -J_1^2(qK)e^{-l^2}. \quad \text{(B2)}$$

Therefore we can assert that the three paths from Fig. 11 must be summed to zero, thus give null contribution to $a_n(0,0+)$.

The remaining Fourier-space paths staying within the region $|m| \leq 1$ are obtained by modifying the last backward step before returning to the origin for each path shown in Fig. 11. In Figs. 11(a) and 11(b) the modification occurs at $(m,q)=(1,-1)$ as shown in Figs. 12(a) and 12(b), and in Fig. 11(c) at $(m,q)=(-1,-1)$ as shown in Fig. 12(c). From the same argument as above it is trivial to see that the contribution to $a_n(0,0)$ from the paths in Fig. 12(b) and 12(c) cancel exactly with those from Fig. 12(a). We note here that, since the paths go through the stationary point twice, the total contribution is enhanced by $\sim K^{-4}$. In this way it can be ascertained that all the Fourier-space paths confined within the region $-1 \leq q \leq 0$ and $|m| \leq 1$, ending at the origin through the position $(m,q)=(1,0+)$, are summed to zero to the K^2 order.

The above logic can be extended to the paths turning to the negative q direction at $(m,q)=(1,-1)$ in Figs. 11(a) and 11(b), or $(m,q)=(-1,-1)$ in Fig. 11(c). It is trivial to see that the contributions sum up to zero in the same way as for Fig. 11 if we note that these paths after turning to the negative q direction must also come back to the stationary point $(m=0,q=-1)$ in order to contribute to $a_n(0,0+)$ to the order K^2. Definitely it must be emphasized that all the dominating Fourier-space paths come back to the origin certainly. Instead of returning to the origin, if the path is halted at a certain point $(0,r)$ along q axis, then the multiplying factor $J_0^n(|r|K)$ is attached to the corresponding path's contribution, thus becomes negligible [8] in the limit of $n \gg 1/(|r|K)^2$. Thus, to the order K^2, the only contribution to $a_n(0,0+)$ is from the paths staying at the origin forever,

$$a_n(m,q)|_{m=0,q=0+} = \frac{1}{4\pi^2}[J_0(qK)e^{-m^2 l^2/2}]^n e^{-iqP_0}e^{-im\varphi_0}$$

$$+ \mathcal{O}(K^4),$$

which is the Eq. (14). We note here that evaluation of $a_n(m,q)|_{m=0,q=0+}$ to the K^2 order has been necessary since the second derivative in q is of order K^2.

[1] B. V. Chirikov, Phys. Rep. **52**, 263 (1979).

[2] A. J. Lichtenberg and M. A. Liebermann, *Regular and Chaotic Dynamics* (Springer-Verlag, Berlin, 1992).

[3] A. J. Lichtenberg and Blake P. Wood, Phys. Rev. Lett. **62**, 2213 (1989).

[4] Gunyoung Park and C. S. Chang, Phys. Rev. E **63**, 066213 (2001).

[5] R. J. Goldston, R. B. White, and A. H. Boozer, Phys. Rev. Lett. **47**, 647 (1981).

[6] Taehoon Ahn and Seunghwan Kim, Phys. Rev. E **49**, 2900 (1994).

[7] J. W. Haus and K. W. Kehr, Phys. Rep. **150**, 264 (1987).

[8] A. B. Rechester, M. N. Rosenbluth, and R. B. White, Phys. Rev. A **23**, 2664 (1981).

[9] C. F. F. Karney, Phys. Fluids **22**, 2188 (1979).

[10] T. M. Antonsen, Jr. and E. Ott, Phys. Fluids **24**, 1635 (1981).